Journal of Fluids and Structures 17 (2003) 603–626

JOURNAL OF FLUIDS AND STRUCTURES

www.elsevier.nl/locate/jnlabr/yjfls

Analysis of aerodynamic problems with geometrically unspecified boundaries using an enhanced Lagrangian method

Dan Mateescu*

Department of Mechanical Engineering, McGill University, Montreal, Que., Canada H3A 2K6

Received 4 March 2002; accepted 25 November 2002

Abstract

This paper presents solutions for several 2-D aerodynamic problems with geometrically unspecified boundaries. These solutions are obtained with an enhanced Lagrangian method based on stream function and Lagrangian-distance coordinates, which includes special procedures to substantially improve the numerical resolution of the shock waves and for the numerical implementation of the aerodynamic conditions defining the geometrically unspecified solid or fluid boundaries. The method is first validated for flows with specified solid boundaries by comparison with exact analytical solutions and with previous computational results obtained by numerical methods using Eulerian formulations. In all cases, this enhanced Lagrangian method displayed a very good accuracy and computational efficiency and a sharp numerical resolution of shock waves. Then this method is used to obtain solutions for problems with geometrically unspecified boundaries, such as: (i) indirect problems of determining the geometrical shape of airfoils and nozzle walls for a specified pressure distribution; (ii) supersonic nozzle design problem for a specified uniform flow at the nozzle outlet based on reflection-suppression condition; (iii) analysis of flexible-membrane airfoils; and (iv) analysis of jet-flapped airfoils.

1. Introduction

The computational methods based on Eulerian representation of the fluid flow, in fixed geometrical coordinates, have been successfully utilized to solve the flow problems past bodies of specified geometrical shapes. However, there are numerous problems of engineering interest in which some of the boundaries of the fluid flow are a priori geometrically unspecified. In these cases, the geometrical shape of these solid or fluid boundaries depends in a certain manner on the flow itself. These types of flow problems are included in the fluid–structure interaction problems.

Examples of such flow problems with geometrically unspecified boundaries are: (i) the indirect flow problems, consisting in the determination of the geometrical shape of an airfoil or wing to generate a specified pressure distribution for a given upstream flow; (ii) analysis of flows past adaptive structures, such as flexible-membrane airfoils or wings, for which the geometrical shape depends on the pressure generated by the fluid flow (or flows past elastic structures subjected to deformations generated by the aerodynamic forces); (iii) design flow problems, in which the geometrical shape of certain solid surfaces in contact with the fluid flow has to be determined to satisfy certain aerodynamic conditions, such as the nozzle design based on the reflection-suppression condition aiming to obtain a specified uniform flow at the nozzle outlet; and (iv) the flow problems with fluid interfaces, such as free surfaces or slip lines, with their geometrical shapes depending on the flow itself; the flows past jet-flapped airfoils or wings, in which the geometrical shape of the thin jet-sheet wake depends on the flow, represent examples for this type of problems.

*Tel.: +1-514-398-6284; fax: +1-514-398-7365.
E-mail address: dan.mateescu@mcgill.ca (D. Mateescu).

0889-9746/03/$ - see front matter © 2003 Published by Elsevier Science Ltd.
doi:10.1016/S0889-9746(02)00162-7

The utilization of the Eulerian flow representation in numerical methods based on fixed grids for such problems with geometrically unspecified boundaries may lead, in most cases, to long iterative procedures eventually requiring computations on successive body shapes until the final geometry is reached.

For this type of problems, the Lagrangian or semi-Lagrangian formulations using streamline coordinates are more suitable, since the geometrically unspecified boundaries are always represented by streamlines. In addition, the Lagrangian formulations may eliminate the need for lengthy grid generation procedures, usually required by the numerical method using Eulerian formulations.

Thus, the Lagrangian formulation based on stream function and Lagrangian-time coordinates, such as that developed by Loh and Hui (1991), eliminates the need for lengthy grid generation procedures. For supersonic flows, this formulation efficiently obtains the solution of the Euler equations by integrating them in Lagrangian time along the streamlines. However, this formulation based on Lagrangian time has discontinuous fluxes across the slip lines and, mathematically, leads to a system of equations which is not fully hyperbolic, being characterized by only five independent eigenvectors, although it has six real eigenvalues (Hui and Zhao, 1993; Yang and Hsu, 1993). These deficiencies can be eliminated by replacing the Lagrangian time with the Lagrangian distance along the streamlines, as shown by Hui and Zhao (1993) and Yang and Hsu (1993). Many studies using Lagrangian formulations have been recently developed by, among others, Loh and Hui (1993), Loh and Liou (1993, 1994), Liou (1995), Strain (1999, 2001), Van Roessel and Hui (1989) and Yang et al. (1993).

In this paper, the generalized Lagrangian formulation based on stream function and Lagrangian distance coordinates is used to obtain solutions for a series of aerodynamic problems involving solid or fluid boundaries of unspecified geometry. In this formulation, the mathematical problem is closed by two compatibility equations associated with the Lagrangian coordinate transformation, which are added to the system of Euler equations of motion, as shown by Loh and Hui (1991), Hui and Zhao (1993), Mateescu and Nasrallah (1995) and Mateescu and Chocron (1996). This augmented system of differential equations is easier to be solved (although it contains two more compatibility equations, which are however simple) since in the Lagrangian coordinates the continuity and energy equations reduce to constants along the streamlines. The numerical strategy consists in the integration in Lagrangian distance (along streamlines) of the augmented system of equations, based on a finite volume discretization, in which the flux values are determined for supersonic flows by using the Riemann problem solution with a Godunov-type scheme, in a similar way as those used by Loh and Hui (1991), Glatz and Wardlaw (1984) and Mateescu and Nasrallah (1995). This Lagrangian method is enhanced by a special procedure developed to substantially improve the numerical resolution of the shock waves, and by special numerical procedures developed for the numerical implementation of the aerodynamic conditions defining the solid or fluid boundaries of unspecified geometry.

The method is first validated for aerodynamic problems with solid boundaries of specified geometry by comparison with exact analytical solutions and with previous computational results obtained by numerical methods using Eulerian formulations. Then this enhanced Lagrangian method is used to determine the solution of several 2-D flow problems with geometrically unspecified boundaries: (i) Determination of the geometrical shape of an airfoil or of a portion of a nozzle wall corresponding to a specified pressure distribution (these are indirect flow problems). (ii) Supersonic nozzle design problem for obtaining a specified uniform flow at the nozzle outlet based on the reflection-suppression condition (design flow problem). (iii) Analysis of supersonic flows past flexible-membrane airfoils (an adaptive-structure type of flow problem). (iv) Analysis of supersonic flows past jet-flapped airfoils (an adaptive fluid boundary problem with slip lines).

In the solution of all these problems this enhanced Lagrangian method displayed an excellent computational efficiency and led to accurate solutions with a sharp numerical resolution of the shock waves and a rigorous treatment of the expansion fans. This method did not require a lengthy grid generation procedure, and was capable of solving very efficiently the flow problems with geometrically unspecified solid or fluid boundaries.

2. Generalized Lagrangian formulation

In the Eulerian representation of the fluid flows, any specific fluid dynamic property, $\pi(\mathbf{r}, t)$, of a fluid particle is a function of time, t, and of its location with respect to a fixed point at that instant of time, represented by the position vector $\mathbf{r} = \mathbf{i}x + \mathbf{j}y + \mathbf{k}z$. In this Eulerian representation, the differential Euler equations of motion governing the steady compressible inviscid (but rotational) flows can be expressed in two-dimensional conservation form as

$$\partial \mathbf{f}/\partial x + \partial \mathbf{g}/\partial y = 0, \quad \mathbf{f} = [\rho u, \rho u^2 + p, \rho uv, \rho H]^{\mathrm{T}}, \tag{1a}$$

$$\mathbf{g} = [\rho v, \rho uv, \rho v^2 + p, \rho H]^{\mathrm{T}}, \tag{1b}$$

where H is the specific enthalpy

$$H = (u^2 + v^2)/2 + (\gamma p/\rho)/(\gamma + 1), \tag{2}$$

in which ρ is the fluid density, p is the pressure, u and v are the components of the fluid velocity, $\mathbf{V} = \mathbf{i}u + \mathbf{j}v$, along the Cartesian coordinates x and y, and γ is the specific heat ratio. The Eulerian representation of the fluid flow has been used on various specified fixed grids to solve mainly flow problems with specified solid boundaries. (for example Anderson et al., 1986; Mateescu, 1990; Mateescu and Venditti, 2001; Roe, 1986).

In the classical Lagrangian representation of the fluid flow, the fluid particles are identified by their location $\mathbf{r}_0 = \mathbf{i}x_0 + \mathbf{j}y_0 + \mathbf{k}z_0$ at a certain time t_0 (called initial time), and any fluid dynamic property at an instant of time t is related to that initial position of the specific fluid particle, that is $\pi(\mathbf{r}_0, t)$. Obviously, this Lagrangian representation implies tracking the motion of a very large number of fluid particles, which would be a very difficult task.

2.1. Lagrangian-time formulation

A more convenient Lagrangian formulation (Loh and Hui, 1991) uses the streamlines and the Lagrangian time, τ (along the streamlines), to identify the fluid particles in their motion. In this Lagrangian formulation, any fluid dynamic property is a function of the value of the stream function ξ (defining the particular streamline) and the Lagrangian time, that is $\pi(\xi, \tau)$. The velocity components are the partial derivatives of the coordinates with respect to the Lagrangian time, $u = \partial x/\partial\tau$ and $v = \partial y/\partial\tau$. The physical coordinates x and y can thus be expressed in function of the Lagrangian time and stream function as

$$\mathrm{d}x = u\,\mathrm{d}\tau + \mathscr{U}\,\mathrm{d}\xi, \quad \mathrm{d}y = v\,\mathrm{d}\tau + \mathscr{V}\,\mathrm{d}\xi, \tag{3}$$

where the derivatives $\mathscr{U} = \partial x/\partial\xi$ and $\mathscr{V} = \partial y/\partial\xi$ of the coordinate transformation have to satisfy the compatibility conditions (since $\mathrm{d}x$ and $\mathrm{d}y$ are total exact differentials): $\partial\mathscr{U}/\partial\tau = \partial u/\partial\xi$ and $\partial\mathscr{V}/\partial\tau = \partial v/\partial\xi$.

For two-dimensional compressible flows, the stream function can be defined in differential form as

$$\mathrm{d}\xi = \rho(u\,\mathrm{d}y - v\,\mathrm{d}x)/K, \tag{4}$$

where K is an a priori constant corresponding to the specific streamline.

In the Lagrangian coordinates τ and ξ, the Euler equations of motion Eq. (1) can be expressed, together with the compatibility relations, in the matrix form

$$\partial\mathbf{E}/\partial\tau + \partial\mathbf{F}/\partial\xi = 0, \tag{5a}$$

$$\mathbf{E} = [K, H, Ku + p\mathscr{V}, Kv - p\mathscr{U}, \mathscr{U}, \mathscr{V}]^{\mathrm{T}}, \tag{5b}$$

$$\mathbf{F} = [0, 0, -pv, pu, -u, -v]^{\mathrm{T}}, \tag{5c}$$

where the specific enthalpy H is defined by (2), and the aforementioned constant K has the expression

$$K = \rho(u\mathscr{V} - v\mathscr{U}). \tag{6}$$

One can notice that the continuity and energy equations, represented by the first two lines of equations (5), are extremely simple and reduce practically to a constant along the streamline. Similarly, the compatibility equations of the coordinate transformation, represented by the last two lines of Eqs. (5), are also very simple. Hence, the system of differential Eqs. (5) is easier to integrate, although it has two more equations than system (1) in the Eulerian formulation. In addition, the Lagrangian formulation is more suitable to solve the flow problems involving boundaries of unspecified geometry, such as the free surfaces, as it will be discussed further. However, this formulation using the Lagrangian time has a deficiency related to the fact that the flux vector $\mathbf{F}$ presents a discontinuity across the fluid interfaces, such as the slip lines, since the tangential velocity component (and hence u and/or v) has different values on the two sides of a slip line. Also, system (5) is not fully hyperbolic, being characterized by only five independent eigenvectors, although it has six real eigenvalues (Hui and Zhao, 1993; Yang and Hsu, 1993).

2.2. Generalized Lagrangian formulation

A generalized Lagrangian formulation based on the stream function, ξ, and the Lagrangian-distance, λ, along the streamlines overcomes the above-mentioned deficiencies (Hui and Zhao, 1993; Yang and Hsu, 1993; Mateescu and Nasrallah, 1995). The Lagrangian distance in this formulation is related to the Lagrangian time by $\mathrm{d}\lambda = V\,\mathrm{d}\tau$, where $V = \sqrt{u^2 + v^2}$ is the magnitude of the fluid velocity. In this case, the coordinate transformation from the physical plane

to the Lagrangian coordinates becomes

$$dx = \cos\theta\, d\lambda + \mathscr{U}\, d\xi, \quad dy = \sin\theta\, d\lambda + \mathscr{V}\, d\xi, \tag{7}$$

where $\theta = \tan^{-1}(v/u)$ is the inclination angle of the fluid velocity, $\boldsymbol{V}$, with respect to the x-axis, and where the derivatives $\mathscr{U} = \partial x/\partial\xi$ and $\mathscr{V} = \partial y/\partial\xi$ of the coordinate transformation have to satisfy the following compatibility relations:

$$\partial\mathscr{U}/\partial\lambda = \partial(\cos\theta)/\partial\xi, \quad \partial\mathscr{V}/\partial\lambda = \partial(\sin\theta)/\partial\xi. \tag{8}$$

The stream function is defined by the same Eq. (4), where K is defined by Eq. (6).

In this Lagrangian formulation, the Euler equations of motion (1) can be expressed, together with the compatibility relations (8), in the matrix form

$$\frac{\partial \mathbf{E}}{\partial\lambda} + \frac{\partial \mathbf{F}}{\partial\xi} = 0, \quad \mathbf{E} = \begin{bmatrix} e_1 \\ e_2 \\ e_3 \\ e_4 \\ e_5 \\ e_6 \end{bmatrix} = \begin{bmatrix} K \\ H \\ Ku + p\mathscr{V} \\ Kv - p\mathscr{U} \\ \mathscr{U} \\ \mathscr{V} \end{bmatrix}, \quad \mathbf{F} = \begin{bmatrix} f_1 \\ f_2 \\ f_3 \\ f_4 \\ f_5 \\ f_6 \end{bmatrix} = \begin{bmatrix} 0 \\ 0 \\ -p\sin\theta \\ p\cos\theta \\ -\cos\theta \\ -\sin\theta \end{bmatrix}, \tag{9}$$

where the specific enthalpy H is defined by Eq. (2). The first two equations in Eq. (9) represent the continuity and energy conservation equations, the next two equations are the projections of the momentum conservation equation on the two axes, and the last two represent the compatibility relations (8) of the coordinate transformation. Each of the first two equations are reduced to a constant along the streamlines, and the last two are again very simple equations. Thus, this system of equations is simpler to integrate than the corresponding system (1) in the Eulerian formulation.

In addition, the free surfaces, such as the slip lines, can be easier treated in this generalized Lagrangian formulation since they are represented by streamlines. Moreover, the flux vector $\mathbf{F}$ does not present any discontinuity across the slip lines, by contrast to the flux $\mathbf{F}$ in the formulation using the Lagrangian time (5) and to the flux $\mathbf{g}$ in the Eulerian formulation (1), which both contain the velocity components that are discontinuous across the slip lines.

As a result, this generalized Lagrangian formulation is more suitable for the analysis of flow problems with geometrically unspecified boundaries, which are always streamlines.

3. Numerical method based on Lagrangian formulation

In this Lagrangian formulation, the aerodynamic problems are solved in a computational domain using a rectangular grid aligned with the Lagrangian coordinates λ and ξ, where the lines $\xi = \xi_j$ = constant represent streamlines, in which subscript j (defining the corresponding streamline) varies from 1 to N_j along the height of the computational domain.

Consider a rectangular cell situated along the streamline $\xi = \xi_j$ and delimited by the streamlines $\xi = \xi_{j-1/2} = \xi_j - \Delta\xi_j/2$ and $\xi = \xi_{j+1/2} = \xi_j + \Delta\xi_j/2$, and by the constant Lagrangian-distance lines $\lambda = \lambda^n$ and $\lambda = \lambda^{n+1} = \lambda^n + \Delta\lambda^n$, where $\Delta\lambda^n$ and $\Delta\xi_j$ define the width and the height of the cell.

The system of equations (9) can be discretized for this cell in the form

$$\mathbf{E}_j^{n+1} = \mathbf{E}_j^n - (\Delta\lambda^n/\Delta\xi_j)(\mathbf{F}_{j+1/2}^{n+1/2} - \mathbf{F}_{j-1/2}^{n+1/2}), \tag{10}$$

where $\mathbf{F}_{j+1/2}^{n+1/2}$ and $\mathbf{F}_{j-1/2}^{n+1/2}$ are the flux values at the cell interfaces aligned to the streamlines. Hence, the numerical strategy adopted here is to integrate the vector $\mathbf{E}$ along λ, from $\lambda = \lambda^1$ (or $n = 1$) to $\lambda = \lambda^N$ (or $n = N$). In fact, the first two components of this vector, K and H, remain constant during this integration, that is $K = K_j$ and $H = H_j$ for the streamline j. For the other components, one needs to calculate first the values of the pressure and the flow velocity inclination, p and θ, at the cell interfaces, since they appear in the flux vector values $\mathbf{F}_{j+1/2}^{n+1/2}$ and $\mathbf{F}_{j-1/2}^{n+1/2}$ at these streamline interfaces.

3.1. Flux calculation based on Riemann problem solution

The flux values at the cell interfaces are calculated for supersonic flows using a procedure based on the solution of Riemann problem, similar to that used in the Godunov method (Loh and Hui, 1991; Glatz and Wardlaw, 1984; Mateescu and Nasrallah, 1995). In this sense, at $\lambda = \lambda^n$ each cell interface along $\xi = constant$, such as that along the streamline $\xi = \xi_{j-1/2}$, is considered to represent a membrane separating two cells of compressible fluid at different states, such as $[\rho_j^n, u_j^n, v_j^n, p_j^n]$ and $[\rho_{j-1}^n, u_{j-1}^n, v_{j-1}^n, p_{j-1}^n]$. This separating membrane is assumed to suddenly disappear for

$\lambda > \lambda^n$ and, as a result, an oblique shock wave and an expansion fan will propagate from the interface into the two neighboring cells, $j-1$ and j. If $p_j^n > p_{j-1}^n$, an oblique shock wave will propagate from the interface into the lower cell $j-1$, and, at the same time, an expansion fan will propagate into the upper cell j, as shown in Fig. 1 (or vice versa if $p_j^n < p_{j-1}^n$).

Denote by θ_{j-1}^n, M_{j-1}^n and θ_j^n, M_j^n the flow inclination angle and the Mach number in the two cells at $\lambda = \lambda^n$, where $M_j^n = \sqrt{[(u_j^n)^2 + (v_j^n)^2]/(\gamma p/\rho)}$, in which $\sqrt{\gamma p/\rho} = a$ represent the local speed of sound. Let also denote by $\theta_{j-1/2}^{n+1/2}$ and $p_{j-1/2}^{n+1/2}$ the flow inclination angle and the pressure at the interface between the two cells, which will result after the generated shock wave and expansion fan. The pressure ratio corresponding to the shock wave is denoted here by $\pi_S = p_{j-1/2}^{n+1/2}/p_{j-1}^n$, and that corresponding to the expansion fan by $\pi_E = p_{j-1/2}^{n+1/2}/p_j^n = \pi_S p_{j-1}^n/p_j^n$.

The inclination angle calculated at the cell interface after the oblique shock wave is

$$\theta_{j-1/2}^{n+1/2} = \theta_{j-1}^n - \tan^{-1}\left[\frac{\pi_S - 1}{\gamma(M_{j-1}^n)^2 - \pi_S + 1}\sqrt{\frac{2\gamma(M_{j-1}^n)^2}{(\gamma+1)\pi_S + \gamma - 1} - 1}\right] \tag{11}$$

and the same inclination angle calculated after the expansion fan is

$$\theta_{j-1/2}^{n+1/2} = \theta_j^n + \nu(M_{j-1/2}^{n+1/2}) - \nu(M_j^n), \tag{12}$$

where the Prandtl–Meyer expansion function, $\nu(M)$, and the Mach number at the interface after the expansion fan, $M_{j-1/2}^{n+1/2}$, are defined as

$$\nu(M) = (1/g)\tan^{-1}\left(g\sqrt{M^2-1}\right) - \tan^{-1}\sqrt{M^2-1}, \tag{13a}$$

$$g = \sqrt{(\gamma-1)/(\gamma+1)}, \tag{13b}$$

$$M_{j-1/2}^{n+1/2} = \left\{[2/(\gamma-1) + (M_j^n)^2]/(\pi_S p_{j-1}^n/p_j^n)^{1-1/\gamma} - 2/(\gamma-1)\right\}^{1/2}. \tag{14}$$

Since the flow inclination angle $\theta_{j-1/2}^{n+1/2}$ and pressure $p_{j-1/2}^{n+1/2}$ at the interface should be the same after both the shock wave and the expansion fan, they can be determined by solving the system of equations (11) and (12). A fast-converging iterative scheme is used in this respect, which starts from an assumed value for π_S.

3.2. Boundary conditions on specified solid walls

Obviously, the above procedure for the flux calculation can be used only for a regular cell situated inside the computational domain. For a cell interface situated along a specified solid wall, the flow inclination angle is known, being equal to the slope angle of the solid wall, such as $\theta_{j-1/2}^{n+1/2} = \theta_{\text{wall}}^{n+1/2}$ (where j can be, for example, $j = 1$ or $j =$

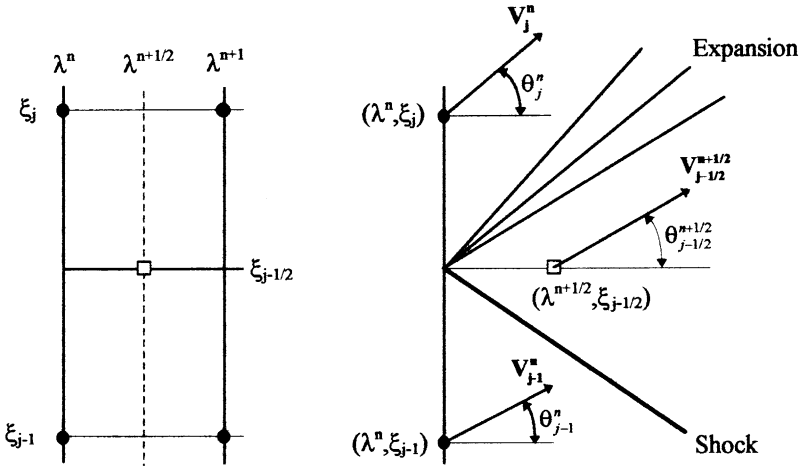

Fig. 1. Representation of the interface $\xi = \xi_{j-1/2}$ between two cells with an illustration of the Riemann problem solution using a Godunov-type scheme.

$N_j + 1$ if the wall is situated along the first or the last streamline of the fluid domain). Thus, only one of the Eqs. (11) or (12) has to be used (depending on the specific situation) to determine the pressure at the corresponding interface.

The treatment of the geometrically unspecified boundaries is discussed in Section 5 for various specific flow problems.

3.3. Determination of primitive flow variables at the step λ^{n+1}

The flux vector calculation requires the values of the pressure and flow direction to be known, and hence the primitive variables have to be calculated after each integration step in λ. Thus, after solving Eq. (10), the components e_i, for $i \in \{1, 2, \ldots, 6\}$, of the vector $\mathbf{E}_j^{n+1}$ are calculated at the step λ^{n+1}, and the corresponding primitive variables can be determined from the following relations:

$$p = \left[e_4\mathscr{U} - e_3\mathscr{V} + \sqrt{(e_4\mathscr{U} - e_3\mathscr{V})^2 + 2(\gamma-1)^2(2K^2H - e_3^2 - e_4^2)}\right]\frac{1}{\gamma+1}\frac{1}{\mathscr{U}^2 + \mathscr{V}^2}, \tag{15}$$

$$u = (e_3 - p\mathscr{V})/K, \quad v = (e_4 + p\mathscr{U})/K, \ \rho = K/(u\mathscr{V} - v\mathscr{U}). \tag{16}$$

$$\theta = \tan^{-1}(v/u), \quad M = \sqrt{(u^2+v^2)/(\gamma p/\rho)}, \tag{17}$$

where $K = e_1$, $H = e_2$, $\mathscr{U} = e_5$, $\mathscr{V} = e_6$. The physical coordinates, x_j^n and y_j^n, for each streamline $\xi = \xi_j$ can be calculated at each step $\lambda = \lambda^n$ by integrating Eqs. (7) for $\xi =$ constant (or $\mathrm{d}\xi = 0$).

3.4. Computational domain discretization. Stability condition

The computational domain is discretized as mentioned into $N \times N_j$ rectangular cells by a number of streamlines, $\xi = \xi_{j-1/2}$ (where j varies from 1 to $N_j + 1$), and by $N + 1$ interface lines $\lambda = \lambda^n$ (where n varies from 1 to $N + 1$). The cell size is defined by $\Delta\xi_j = \xi_{j+1/2} - \xi_{j-1/2}$ and $\Delta\lambda^n = \lambda^{n+1} - \lambda^n$.

The steps $\Delta\xi_j$, which represent the mass flow rate between the two streamline interfaces, are determined from the fluid flow parameters at the inlet. For a uniform flow at the inlet defined by the velocity U_∞ inclined at an angle α with respect to x-axis, the density ρ_∞, and static pressure p_∞, the physical distance between the streamlines is assumed uniform, $\Delta h = \Delta y/\cos\alpha = \Delta x/\sin\alpha$, and hence the size of $\Delta\xi_j$ increments are uniform

$$\Delta\xi_j = \Delta\xi = \rho_\infty U_\infty \Delta y/\cos\alpha = \rho_\infty U_\infty \Delta x/\sin\alpha. \tag{18}$$

The initial flow parameters at $\lambda = \lambda^1 = 0$ needed to start the integration process can thus be obtained as

$$u_\infty = U_\infty \cos\alpha, \quad v_\infty = U_\infty \sin\alpha, \tag{19}$$

$$\mathscr{U}_\infty = \partial x/\partial\xi\big|_{\lambda=0} = \sin\alpha/(\rho_\infty U_\infty), \tag{20a}$$

$$\mathscr{V}_\infty = \partial y/\partial\xi\big|_{\lambda=0} = \cos\alpha/(\rho_\infty U_\infty), \tag{20b}$$

$$K_\infty = \rho_\infty(u_\infty\mathscr{V}_\infty - v_\infty\mathscr{U}_\infty), \tag{21a}$$

$$H_\infty = U_\infty^2/2 + (p_\infty/\rho_\infty)/(1 - 1/\gamma), \tag{21b}$$

$$e_{3\infty} = K_\infty u_\infty + p_\infty\mathscr{V}_\infty, \tag{22a}$$

$$e_{4\infty} = K_\infty v_\infty - p_\infty\mathscr{U}_\infty. \tag{22b}$$

The integration step $\Delta\lambda^n$ has to satisfy the stability condition, which can be expressed as

$$\Delta\lambda^n = CFL\,\Delta\xi_j/[2\rho_j u_j \tan(\theta_j + \mu_j)], \tag{23}$$

where θ_j is the flow direction angle, $\mu_j = \sin^{-1}(1/M_j)$ is the Mach angle, and CFL represents the Courant–Friedrich–Levy number, which should be taken smaller than 1 in this case. The derivation of this stability condition is based on the theory of characteristics.

3.5. Improved shock resolution procedure

When the slope of the body surface has a sudden compression-type change, a stronger shock wave can be generated at that location. In this case, an arbitrary value of the integration step, $\Delta\lambda^n$ (chosen to satisfy the stability condition),

usually leads to significant numerical errors and to the inability of capturing sharp shocks without numerical distortions, as shown in Section 4.1 (Fig. 4). This type of loss of accuracy has also been observed by Loh and Hui (1993) who used a local analytical solution at the location of the slope change, similar to that used by Glatz and Wardlaw (1984) for a Godunov scheme.

In the following, we will use a different procedure by conveniently adjusting the Lagrangian-distance increment $\Delta\lambda^n$. First, the integration step $\Delta\lambda^{n-1}$ is adjusted such that the Lagrangian-distance line $\lambda = \lambda^n$ coincides with the location of the wall slope change. However, this is not enough to solve this difficulty. As shown in Fig. 2a in a physical plane representation, the cell interface along the line $\lambda = \lambda^{n+1}$ is normally divided by the shock wave into two parts, one part situated in the uniform flow field upstream of the shock and the other in the flow field downstream of it. This state discontinuity along this interface was found to be at the root of the numerical errors. By adjusting the size of the integration step $\Delta\lambda^n$ to avoid this discontinuity, as shown in Fig. 2b, the solution accuracy is substantially improved. This step adjustment is calculated using the equation $\Delta\lambda = \Delta\xi J \sin\beta/\sin(\sigma - \beta)$, where J is the Jacobian of the coordinate transformation, $\sigma = (\mathscr{U}\cos\theta + \mathscr{V}\sin\theta)/(\mathscr{U}\sin\theta - \mathscr{V}\cos\theta)$ and β represents the oblique shock angle, which can be determined in the process of flux calculation discussed in Section 3.1. It is worth noting that this adjusted step $\Delta\lambda^n$ may not always be consistent with the CFL stability condition (23), but this has no negative effects on the numerical stability, as long as the stability condition is again satisfied after the jump $\Delta\lambda^n$. A representation in the physical plane of the resulting adjusted grid is shown in Fig. 2c.

As shown in Sections 4.1 and 4.3, this improved numerical procedure has led to an excellent accuracy of the numerical solution, in which the numerical representation of the shock waves is very accurate and sharp.

4. Solutions of flow problems with specified solid boundaries

Before using it for the analysis of flow problems with geometrically unspecified boundaries, this Lagrangian method has been first applied for validation to the study of several flow problems with specified solid boundaries.

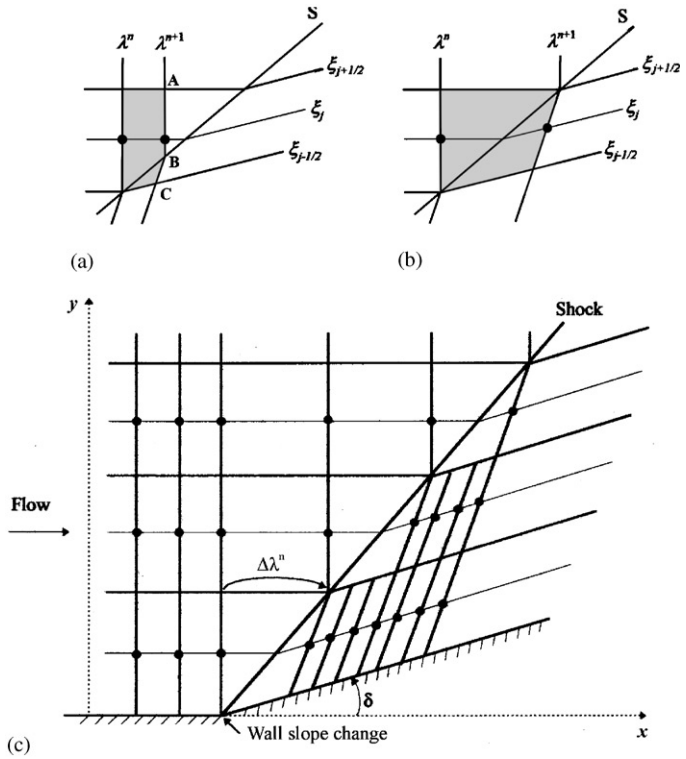

Fig. 2. Illustration of the numerical procedure to improve the shock resolution.

4.1. Flow in a duct with multiple shock reflections. method validation

The supersonic flow in a duct with a lower wall suddenly deflected by an angle δ is shown schematically in Fig. 3a. The oblique shock wave on the lower wall is successively reflected on the upper and the lower walls. Numerical computations have been performed for this problem considering an inlet duct height $h_{in} = 1$, an inlet Mach number $M_{in} = 2$ and a wall deflection angle $\delta = 7^\circ$. A number of 61 streamlines have been considered across the duct height.

The numerical solutions obtained with the present Lagrangian method using the improved shock resolution procedure (discussed in Section 3.5), and without it (see Mateescu and Nasrallah, 1995) are compared in Fig. 4 with the exact analytical solutions for the 1st and the 21st streamlines in the region of the wall deflection location (upstream and downstream of the first shock). It was found that the present Lagrangian method with the improved shock resolution procedure displays a very good resolution of the shock waves, with sharp discontinuities and highly accurate results. This can also be seen in Table 1 for the first two reflected shocks in terms of the corresponding Mach numbers and shock locations. The agreement shown in this table between the present solution and the exact analytical solution is remarkable.

The complete Mach number and pressure distributions obtained with the present Lagrangian method are shown in Fig. 5, for the closest streamlines to the lower and upper walls (streamlines 1 and 61, respectively) and for five intermediate streamlines (streamlines 11, 21, 31, 41 and 51). The streamline pattern of this flow is shown in Fig. 3b, in which the shock waves are clearly indicated by the changes of the streamline slopes (the scale of y-axis is enlarged with respect to that of x-axis).

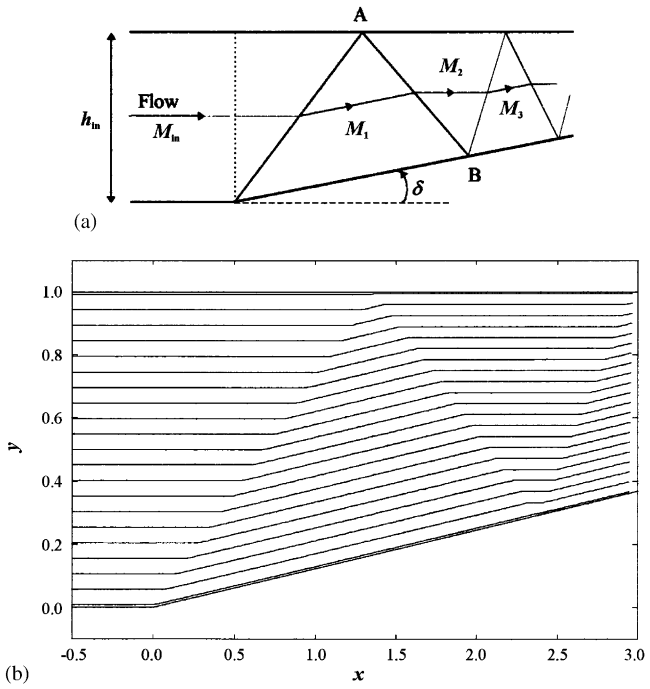

Fig. 3. (a) Geometry of the supersonic flow in a duct with multiple shock reflections. (b) Streamline pattern of this flow.

Table 1
Comparison between the present solution and the exact analytical results for a duct flow with multiple shock reflections

	Initial shock	First reflected shock (A)		Second reflected shock (B)	
	M_1—Mach number	M_2—Mach number	x_A—Shock location	M_3—Mach number	x_B—Shock location
Present solution	1.7498	1.5088	1.3977	1.2589	2.4091
Exact analytical solution	1.7498	1.5088	1.3976	1.2588	2.4093

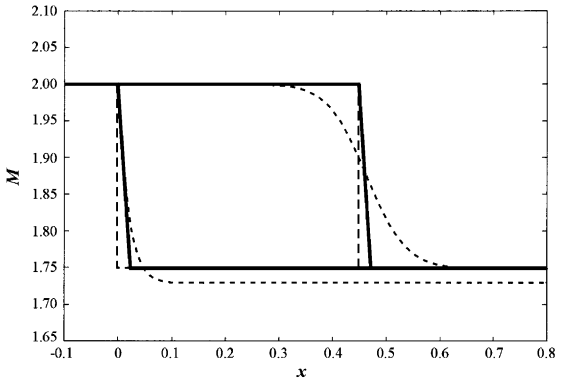

Fig. 4. Variation of the Mach number along the 1st and 21st streamlines in the region of the wall deflection location ($x = 0$). Comparison between: ——, present Lagrangian solution with improved shock resolution procedure; - - -, Lagrangian solution without improved shock resolution procedure; – – – , exact analytical results.

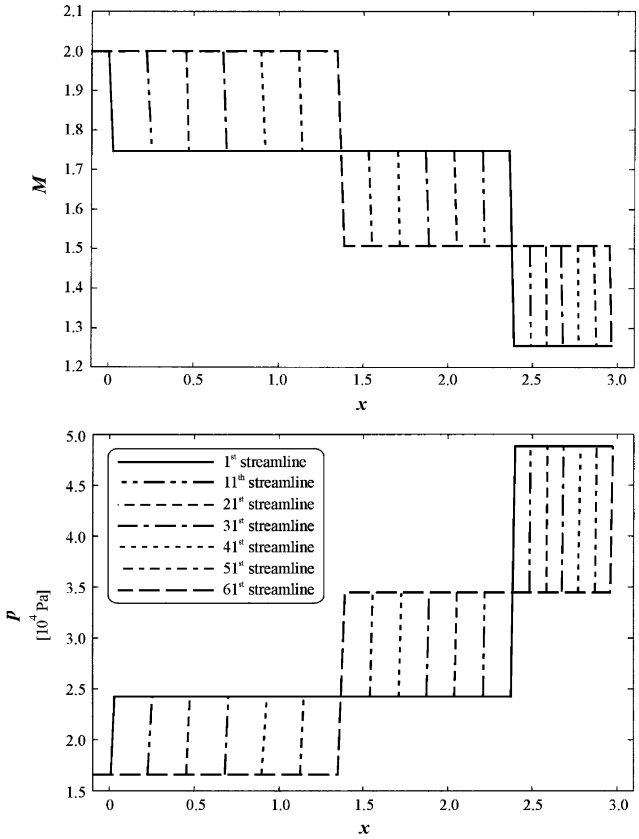

Fig. 5. *Supersonic flow in a duct with multiple shock reflections.* Mach number and pressure distributions along seven streamlines: ———, 1st streamline (closest to the lower wall); — - - —, 11th streamline; – – –, 21st streamline; — - —, 31st streamline; - - - -, 41st streamline; – - – - –, 51st streamline; — —, 61st streamline (closest to the upper wall).

4.2. Flow in a duct with a shock and an expansion on the lower wall

Computations have also been performed for the supersonic flow in a duct with a straight wedge of length $l = h_{in} = 1$, shown schematically in Fig. 6a. The geometry of the first part of the duct was the same as in Section 4.1, with $\delta = 7^\circ$ and $M_{in} = 2$, but at the end of the wedge the lower wall becomes again parallel to the upper wall through a deflection

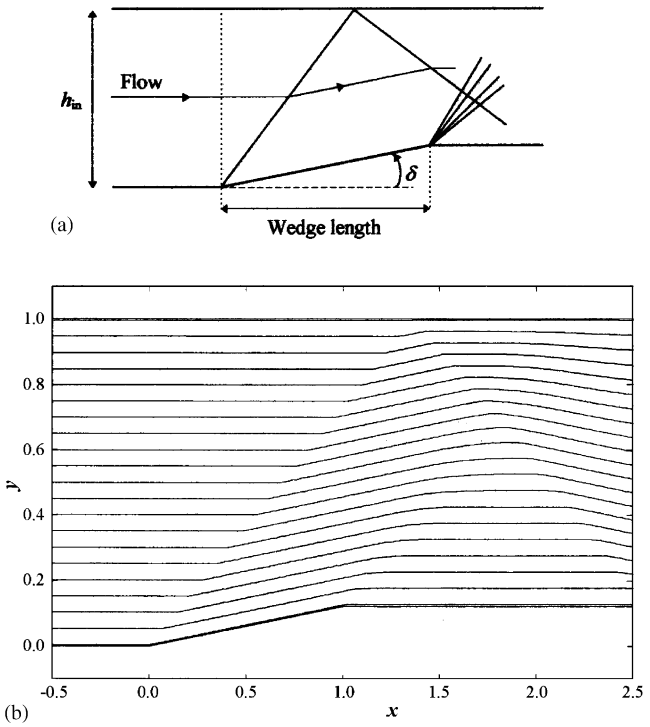

Fig. 6. (a) Geometry of the supersonic flow in a duct with a shock and an expansion fan at the lower wall. (b) Streamline pattern of this flow.

with the same angle, $\delta = 7^\circ$, but in the opposite sense. This test was done to validate this method for the Prandtl–Meyer expansion fan generated at the downstream corner of the wedge. The present solution was found in good agreement with the exact analytical results obtained for the Prandtl–Meyer expansion, without any special numerical treatment of the expansion fan.

The streamline pattern of this flow is shown in Fig. 6b, and the Mach number and pressure distributions for seven streamlines are shown in Fig. 7.

4.3. *Flow in a circular-arc nozzle: method validation*

This flow problem in a duct with a circular-arc bump of length $l_B = h_{in} = 1$ and height $h_B = 0.04h_{in}$, shown schematically in Fig. 8a, has been previously studied, among others, by Eidelman et al. (1984), Ni (1982) and Mateescu and Stanescu (1995) using different numerical methods based on Eulerian formulations. The present solution for the Mach number distribution, obtained for $M_{in} = 1.65$ using 81 streamlines, is compared in Fig. 9a, for validation, with the results obtained by Eidelman et al. (1984) for the closest streamlines to the lower and upper walls (1st and 81st streamlines, respectively). Good agreement was found between these solutions, with the observation that the shock wave resolution is slightly sharper in the present solution. The Mach number distribution along three other intermediate streamlines (21st, 41st and 61st) is also shown in Fig. 9 (comparison not available). The pressure distributions along these five streamlines are also shown in Fig. 9. The pressure distribution calculated on the circular-arc bump will be used as an input in Section 5.2 for the indirect flow problems with specified pressure distribution. The streamline pattern of this flow is shown in Fig. 8b (again the scale of y-axis is enlarged with respect to that of x-axis).

It is worth noting that the same flow problem has also been solved (again for validation purpose) on the same type of PC, by a biased-flux method based on a finite volume formulation developed by Mateescu and Stanescu (1995), which uses an Eulerian representation of the flow. The computing time required by the present Lagrangian method was almost one order of magnitude smaller than that method based on the Eulerian flow representation for the same accuracy, although that particular method was itself characterized by a high computational efficiency in comparison with other

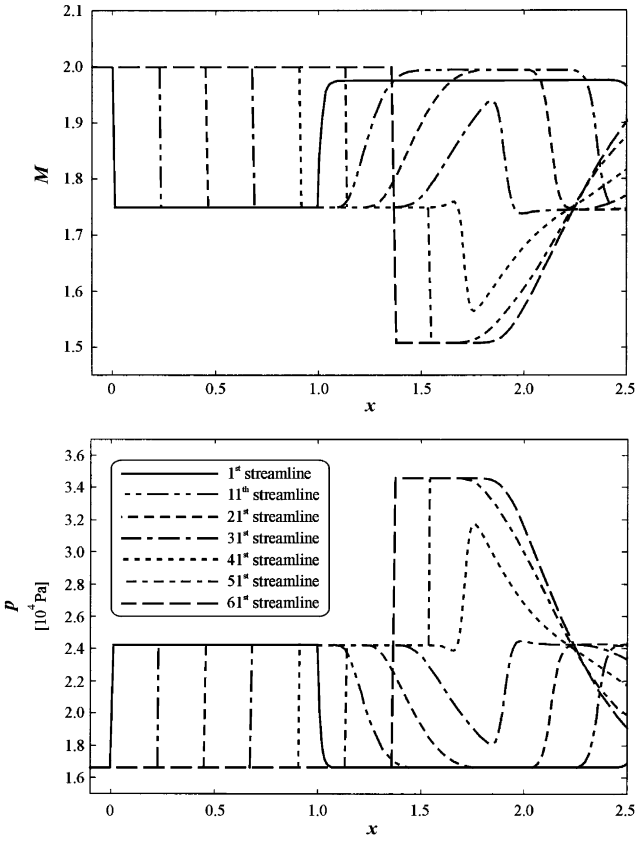

Fig. 7. *Supersonic flow in a duct with a shock and an expansion fan at the lower wall.* Mach number and pressure distributions along seven streamlines: ———, 1st streamline (closest to the lower wall); — - - —, 11th streamline; – – –, 21st streamline; — - —, 31st streamline; - - - -, 41st streamline; – - – - –, 51st streamline; — —, 61st streamline (closest to the upper wall).

Eulerian methods (such as Jameson's method as mentioned in that paper). This shows the advantages of the present Lagrangian method for the flow problems which can be treated in this manner.

4.4. Flow in a supersonic parabolic nozzle

The geometry of this nozzle consists in two parabolas smoothly connected at the midpoint of the nozzle length, as shown in Fig. 10a. Due to the nozzle symmetry, only the lower half of the nozzle will be considered in the computations, the axis of symmetry acting as a solid boundary.

Computations have been performed for the inlet and outlet cross-sectional heights $h_{in} = 1$ and $h_{\text{out}} = 4$ (hence area ratio $h_{\text{out}}/h_{in} = 4$), the nozzle length $l_{\text{noz}} = 20$ and the inlet Mach number $M_{in} = 1.05$. A number of 15 streamlines has been used in this case.

The expansion waves generated in the expansion portion of the nozzle are subjected to successive multiple reflections on the upper and lower walls, which generate oscillations of the flow variables along the nozzle, including oscillations of the flow direction and Mach number. As a result, the flow parameters in a cross-section are strongly nonuniform. In order to study the axial evolution of these oscillations, the computational domain was extended with a uniform cross-section of an additional length of 100 times the inlet height, or five times the nozzle length (that is $l_{\text{comp}} = 120$).

The results obtained for this nozzle flow will be compared with those obtained in the nozzle design problem studied in Section 5.2, which aims to obtain a uniform flow at the nozzle exit.

The Mach number and pressure distributions along five streamlines (1st, 5th, 8th, 11th and 15th) are shown in Fig. 11. One can notice that the Mach number has a very large cross-sectional variation at the nozzle exit, and its oscillations continue to exist at long distances from the nozzle exit in spite of a very smooth variation of the nozzle

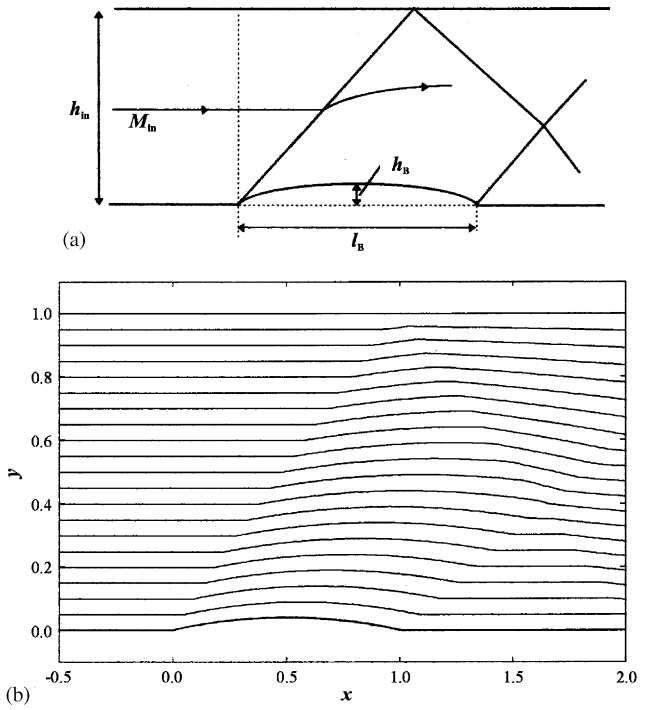

Fig. 8. (a) Geometry of the circular-arc nozzle. (b) Streamline pattern of this flow.

geometry and its very long extension of constant cross-section. As shown in Fig. 11, these oscillations are not completely damped even after a distance of 5 times the nozzle length.

The streamline pattern, indicating the oscillations in the flow direction, is shown in Fig. 10b (please note that the y-axis is very much enlarged in this figure in comparison with the x-axis).

4.5. Flow past a lenticular airfoil at incidence

This symmetric airfoil of chord c, with the upper and lower surfaces represented by two circular arcs, is placed at an incidence α in a uniform flow of Mach number M_∞. Computations have been performed with this Lagrangian method for an airfoil maximum thickness $th = 0.04c$, with $\alpha = 7^\circ$ and $M_\infty = 2$, considering 120 streamlines (60 on each side of the airfoil). The Mach number and pressure distribution on the closest streamlines to the upper and lower surfaces are shown in Fig. 12. The streamline pattern of the flow past this airfoil is shown in Fig. 13.

The pressure distribution calculated on this airfoil will be used as an input in Section 5.1 for the indirect flow problems with specified pressure distribution.

5. Solutions of flow problems with geometrically unspecified boundaries

The flow problems of unspecified geometry require a special treatment of the geometrically unspecified boundaries. This will be illustrated in the following for several types of specific flow problems.

5.1. Indirect flow problems with specified pressure distribution: method validation

In the case of indirect flow problems in which the solid boundary (or a portion of it) is defined by a specified pressure distribution, this Lagrangian method can be directly used without many modifications. Thus, for these problems, the specified pressure on the wall is imposed at the boundary in the process of flux calculation, that is $p_{j-1/2}^{n+1/2} = p_{\text{spec}}^{n+1/2}$, instead of imposing the flow inclination angle $\theta_{j-1/2}^{n+1/2}$ at the solid wall. Then $\theta_{j-1/2}^{n+1/2}$ is determined in the process of flux calculation (based on the Riemann problem solution) indicated in Section 3.2, and the final flow variables, including the

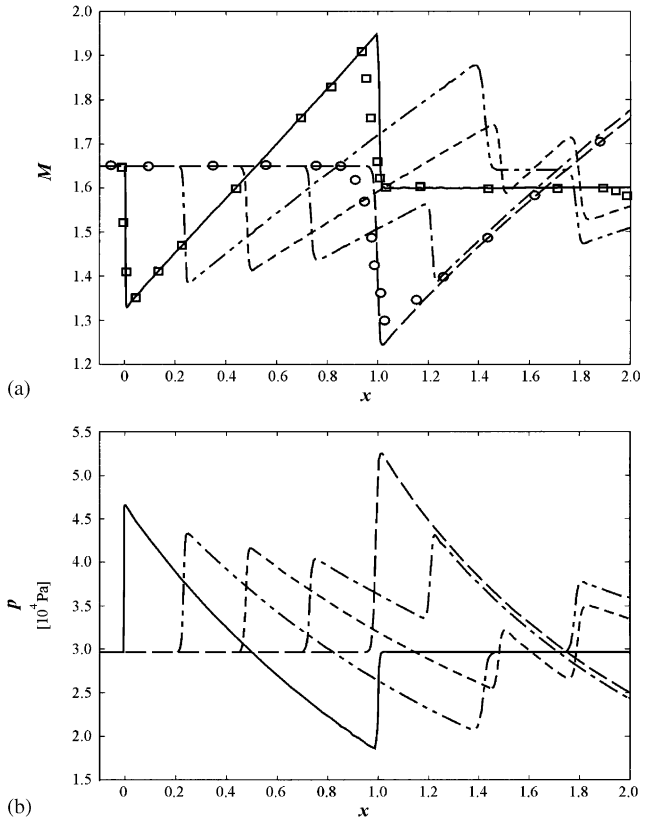

Fig. 9. *Supersonic flow in a circular-arc nozzle*. Present Lagrangian solution for the Mach number and pressure distributions along five streamlines: ———, 1st streamline (closest to the lower wall); — - - —, 21st streamline; – – –, 41st streamline; — - —, 61st streamline; — —, 81st streamline (closest to the upper wall). Comparison with the numerical results obtained by Eidelman et al. for the Mach number distribution on the lower wall (⊠) and on the upper wall (○).

flow inclination angle at the wall θ_j^{n+1} at the next Lagrangian-distance line $\lambda = \lambda^{n+1}$ (and hence the wall geometry), are calculated from Eq. (10) as indicated in Section 3.

5.1.1. Indirect problem of a nozzle with specified wall pressure distribution

The pressure distribution determined in Section 4.3 on the circular-arc bump is now considered as being specified (as input) on the portion $0 < x < l_B$ of the duct wall, where $l_B = h_{in} = 1$ (obviously, the wall geometry is not specified on this portion). The geometrical shape of the duct wall with specified pressure distribution is obtained by solving this indirect flow problem as indicated in Section 5.1. The resulting geometrical shape of the duct wall is compared for validation in Fig. 14a with the original circular-arc shape, initially used in Section 4.3 to determine the pressure distribution used here as input. A numerical comparison of the y-coordinates computed in the indirect flow problem and those of the original wall considered in the direct problem (as input) is shown in Table 2 for the points indicated in Fig. 14a. One can notice a very good agreement between these coordinates, which indicate an excellent accuracy of the solution of the indirect flow problem with specified pressure distribution.

5.1.2. Indirect problem of an airfoil with specified pressure distribution

Similarly, the pressure distribution determined in Section 4.5 on the lenticular airfoil is now considered as being specified (as input). The resulting geometrical shape of the airfoil is compared for validation in Fig. 14b with the original geometry of the airfoil initially used in Section 4.5 to determine the pressure distribution used here as input. A numerical comparison of the y-coordinates computed in the indirect flow problem and those of the original lenticular airfoil considered in the direct problem is shown in Table 2 for the points indicated in Fig. 14b, which indicate an excellent accuracy of the solution of the indirect flow problem with specified pressure distribution.

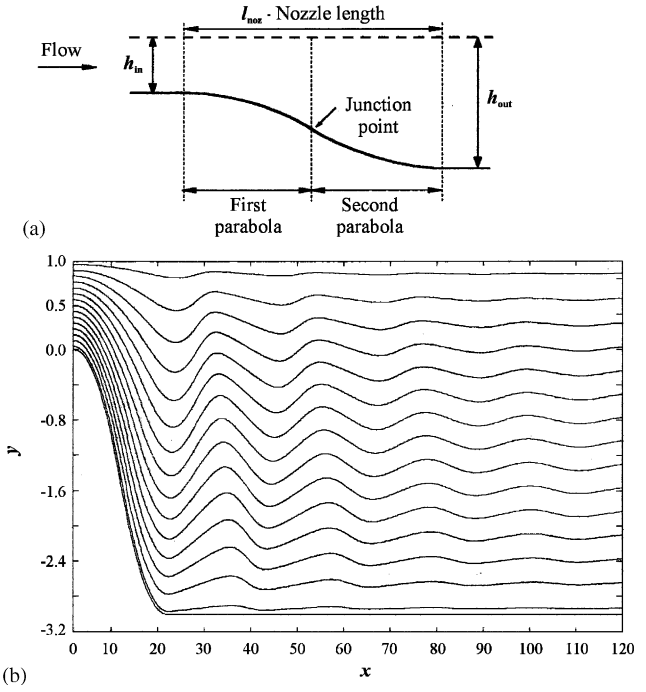

Fig. 10. (a) Geometry of the parabolic supersonic nozzle. (b) Streamline pattern of this flow.

5.2. *Nozzle design problem*

This enhanced Lagrangian formulation has proven suitable and very efficient in solving the design flow problems, such as that of the design of the geometrical shape of a supersonic nozzle to obtain a uniform flow of a specified Mach number at the exit, M_{out}.

As shown in Section 4.4, the expansion waves generated in the expansion portion of the nozzle are subjected to successive multiple reflections on the lower and upper walls, which generate strong oscillations of the flow variables along the nozzle and in its extension. Figs. 10b and 11 show these oscillations for the flow inclination angle, Mach number and pressure, which continue long after the nozzle outlet ($l_{\text{noz}} = 20h_{in}$) in its extension with a length of 100 times the inlet height.

In order to obtain a uniform flow at the nozzle exit, the successive expansion wave reflections have to be eliminated by using a reflection-suppression boundary condition at the nozzle wall. This is achieved by imposing the wall slope to follow the shape of the closest streamline to the wall, that is $\theta_{\text{wall}}^{n+1} = \theta_j^{n+1}$, where $j = 1$ was taken as the closest streamline to the lower wall in the present computations.

The solution of the nozzle design problem is illustrated here for the case studied by Anderson (1991), aiming to obtain a uniform flow at the nozzle outlet of Mach number $M_{\text{out}} = 2.4$. Computations have been performed for the lower half of the nozzle (due to the nozzle symmetry), with the inlet Mach number $M_{in} = 1.001$, inlet height $h_{in} = 1$ and a number of 211 streamlines. A very short circular arc has been considered in this case at the inlet in order to avoid the flow separation that may be caused by a very sharp corner expansion and the wall slope at the end of this circular arc was calculated as $\theta_{wm} = [\nu(M_{in}) - \nu(M_{\text{out}})]/2$.

The designed geometrical shape of the nozzle and the streamline pattern of the flow are shown in Fig. 15, together with the variation of the Mach number along five streamlines (1st, 61st, 106th, 166th, 211th). One can notice a very smooth variation of the flow inclination angle along the streamlines, and a very efficient stabilization of the Mach number variation along the nozzle (by contrast to the situation shown in Figs. 10b and 11 in the case of the parabolic nozzle). The outlet to inlet area ratio was found to be $h_{\text{noz}}/h_{in} = 2.3958$, which is in good agreement with the value of 2.403 obtained by Anderson (1991) using the method of characteristics (the slight difference can be attributed to the slight difference in the inlet conditions).

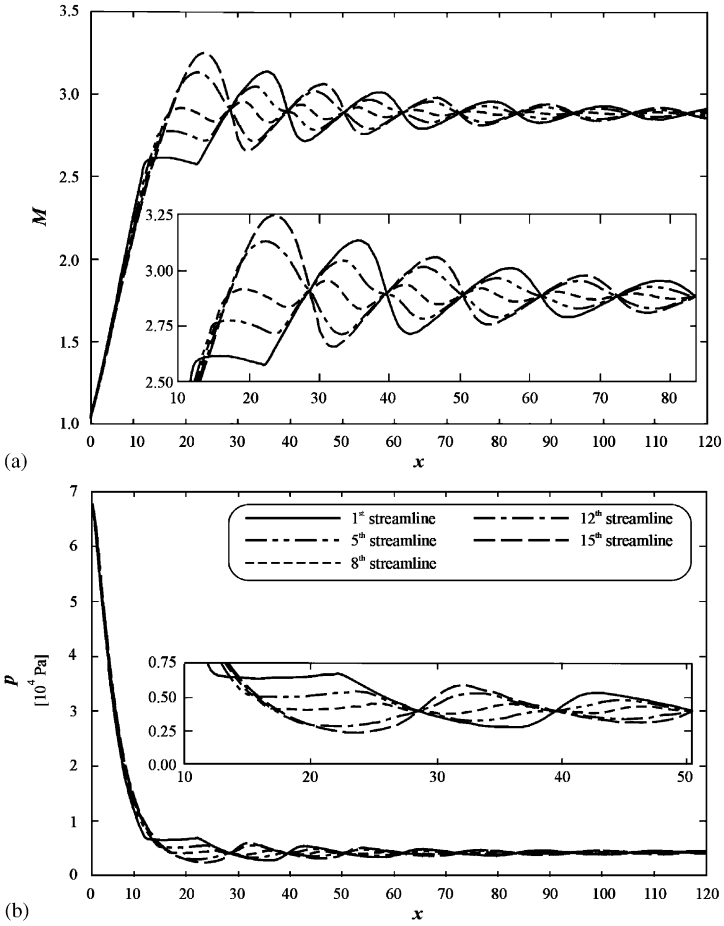

Fig. 11. *Supersonic flow in a parabolic nozzle*. Mach number and pressure distributions along five streamlines: ———, 1st streamline (closest to the lower wall); — - - —, 5th streamline; – – –, 8th streamline; — - —, 12th streamline; — —, 15th streamline (closest to the upper wall).

5.3. *Analysis of flexible-membrane airfoils*

Another types of flow problems with geometrically unspecified boundaries are those resulting from the consideration of the structural deformations of the aerodynamic surfaces (static aeroelasticity problems) or the adaptive structures. The present enhanced Lagrangian method has proven to be very efficient also for solving this type of problems. This is illustrated here for flexible-membrane airfoils in supersonic flow, in which case the geometrical shape of the membrane depends on the pressure difference across it (see Mateescu and Newman, 1991, for the subsonic case). In order to validate the Lagrangian solution, an analytical solution is derived first for this problem.

5.3.1. *Analytical solution*

Consider a flexible-membrane airfoil of chord c with the leading and trailing edges situated on the x-axis of a Cartesian coordinate system, and denote by α its incidence with respect to the velocity U_∞ of a uniform stream in which it is placed. The pressure difference coefficient across this thin airfoil can be obtained, using the method indicated in Carafoli et al. (1969) and Mateescu (1987), in the form

$$\Delta C_p = (4/B)(\sin\alpha - \cos\alpha \tan\theta), \quad B = \sqrt{M_\infty^2 - 1}, \tag{24}$$

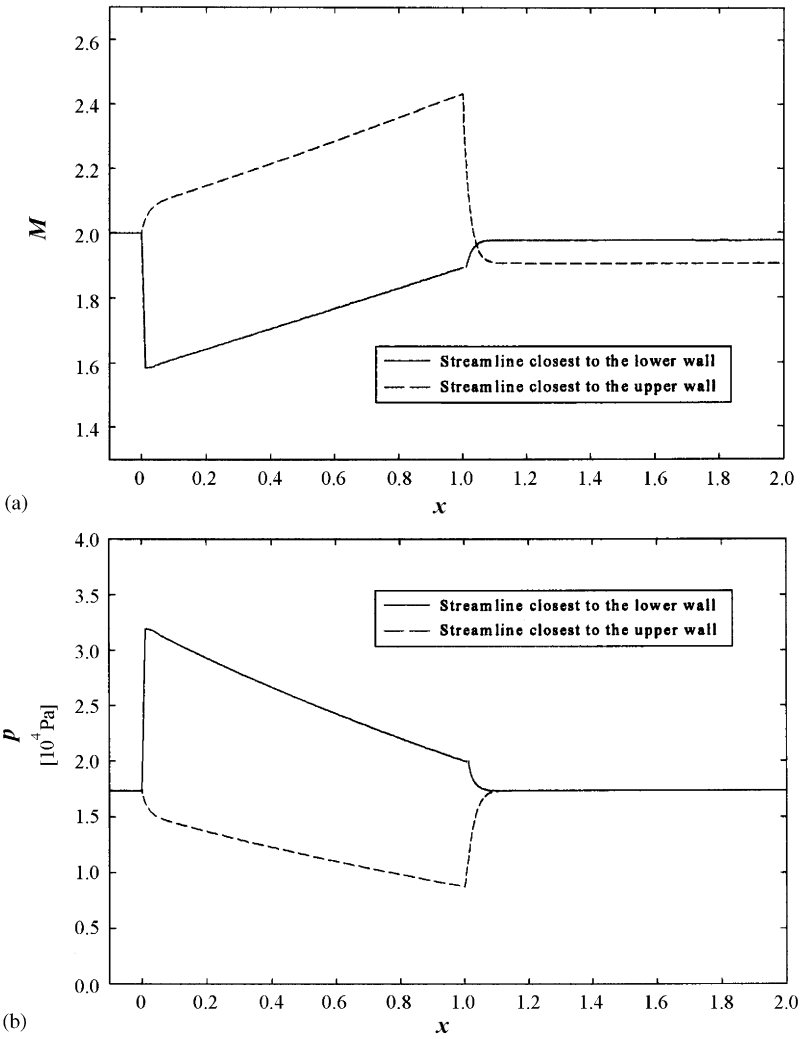

Fig. 12. *Lenticular airfoil*. Mach number and pressure distributions along two streamlines: ———, closest streamline to the lower wall; – – –, closest streamline to the upper wall.

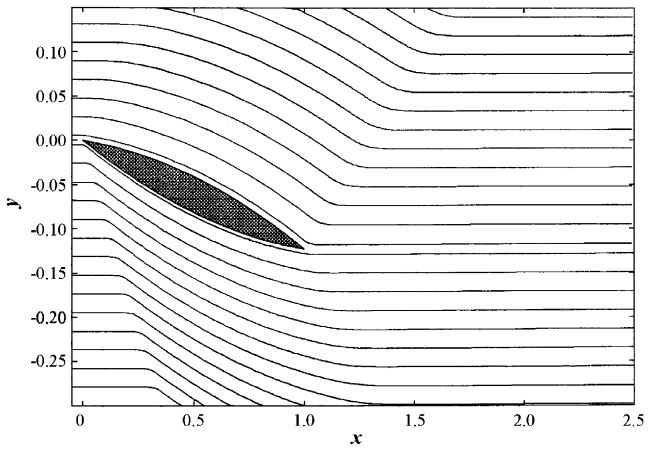

Fig. 13. *Lenticular airfoil*. Streamline pattern of the flow.

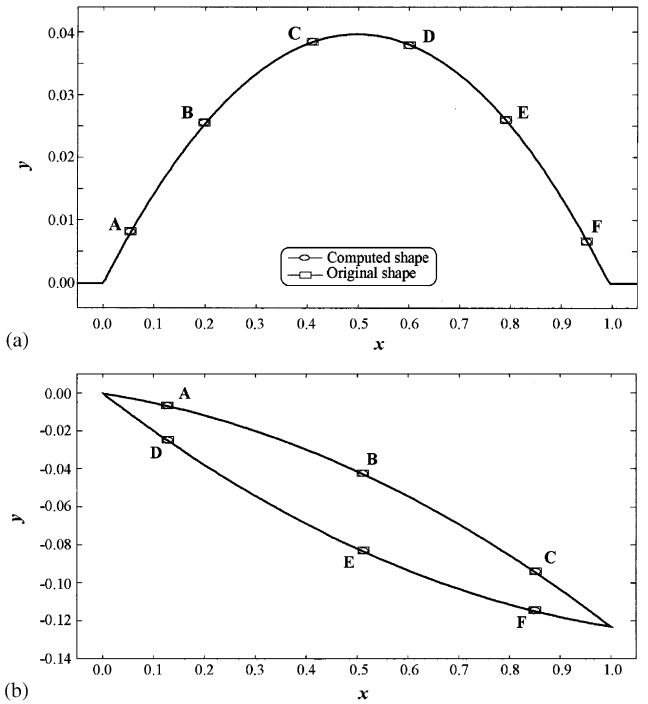

Fig. 14. *Indirect flow problem.* (a) Indirect nozzle problem and (b) indirect airfoil problem. Comparison between: Computed wall geometry for a specified pressure distribution (—○—); Original geometry used to calculate the pressure distribution serving as input in the indirect problem (—□—).

Table 2
Computed geometry of the indirect flow problems with specified pressure distribution. Method validation by comparison with the original geometry used to determine the pressure distribution serving as input in the indirect method

y-Coordinate	Indirect nozzle problem with specified pressure distribution		Indirect airfoil problem with specified pressure distribution	
	Computed geometry	Original geometry	Computed geometry	Original geometry
Point A	0.00761	0.00761	−0.0082	−0.0082
Point B	0.02601	0.02602	−0.0429	−0.0430
Point C	0.03825	0.03826	−0.0938	−0.0937
Point D	0.03785	0.03787	−0.0288	−0.0291
Point E	0.02547	0.02549	−0.0833	−0.0835
Point F	0.00656	0.00658	−0.1143	−0.1146

where M_∞ is the Mach number of the uniform stream and θ denotes here the local slope angle of the flexible-membrane airfoil, which is a priori unknown. This slope angle is in fact related to the pressure difference and the tension in the membrane by the equilibrium equation normal to the membrane, as shown in Mateescu and Newman (1991). This equation can be expressed as

$$\Delta C_p = -cC_T\left[\mathrm{d}(\tan\theta)/\mathrm{d}x\right], \quad C_T = 2T/(\gamma M_\infty^2 p_\infty c), \tag{25}$$

where C_T is the nondimensional tension coefficient, which leads to the linear differential equation

$$\frac{\mathrm{d}\theta}{\theta-\alpha} = \frac{1}{cC_T}\frac{4}{B}\mathrm{d}x. \tag{26}$$

After integration one obtains

$$\theta - \alpha = (\theta_0 - \alpha)\exp(Ax/c), \quad A = 4/(BC_T). \tag{27}$$

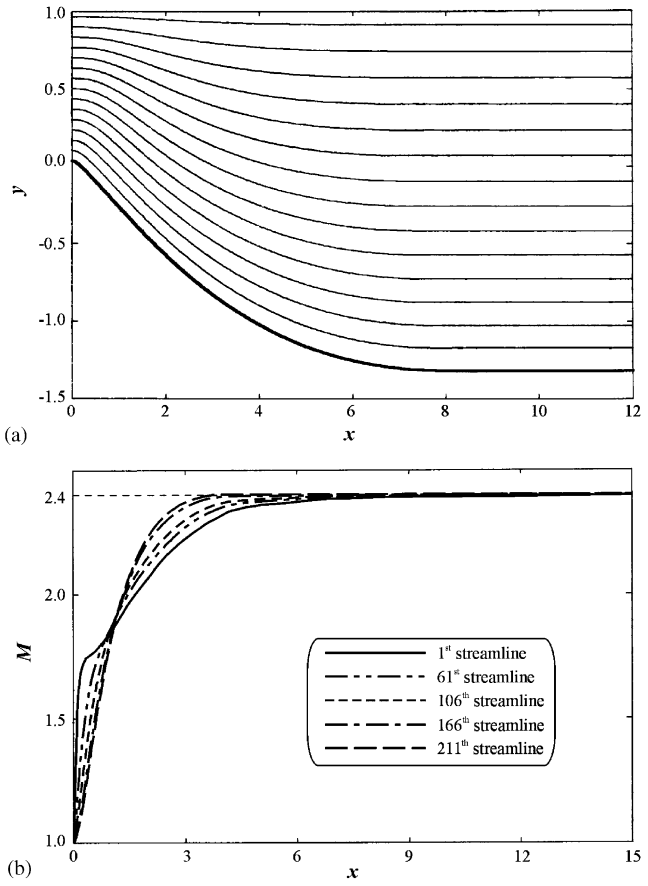

Fig. 15. *Nozzle design problem.* (a) Designed geometrical shape of the nozzle and the streamline pattern of the flow and (b) Mach number distribution along five streamlines: ———, 1st streamline (closest to the lower wall); — - - —, 61st streamline; – – –, 106th streamline; — - —, 166th streamline; — —, 211th streamline (closest to the upper wall).

Since the slope angle $\theta = \tan^{-1}[h'(x)]$ is defined in function of the membrane shape equation $y = h(x)$, one obtains after another integration the geometrical shape of the membrane in the form

$$h(x) = \alpha x + c\big[(\theta_0 - \alpha)/A\big][\exp(Ax/c) - 1], \tag{28a}$$

$$\theta_0 = \alpha[1 - A/(\exp A - 1)]. \tag{28b}$$

The excess length ε of the membrane with respect to its chord, defined by

$$\varepsilon = \ell/c - 1 = (1/c)\int_0^c \sqrt{1 + [h'(x)]^2}\,\mathrm{d}x - 1, \tag{29}$$

where ℓ is the membrane length, which can be approximately calculated as

$$\varepsilon = (\alpha^2/4)[A(\exp(2A) - 1)/(\exp A - 1)^2 - 2]. \tag{30}$$

5.3.2. Lagrangian method solution

In this case, the implementation of the boundary condition on the membrane should include the equilibrium equation normal to the membrane, which can be expressed for numerical use as

$$\Delta\theta = 2\sin^{-1}\left(-\frac{\Delta p}{2T}\Delta\lambda\right), \quad \Delta\lambda = \lambda^{n+1} - \lambda^n, \tag{31}$$

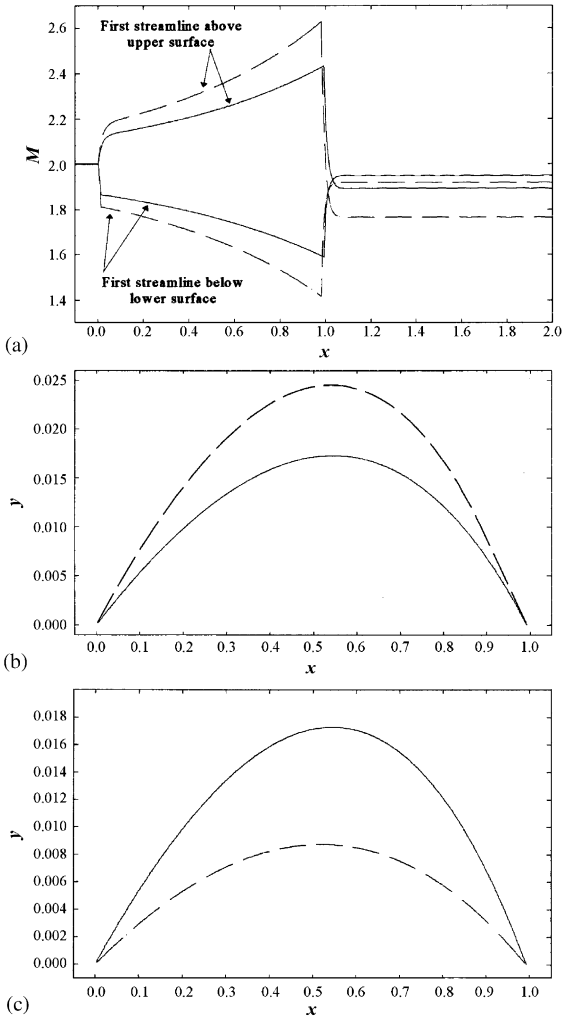

Fig. 16. *Flexible-membrane airfoil*. (a) Mach number distributions along the closest streamlines to the lower and upper surface for $M_\infty = 2$, $C_T = 2$ and for two values of the incidence: ———, $\alpha = 7^\circ$; — — $\alpha = 10^\circ$. (b) Geometrical shape of the membrane for $M_\infty = 2$, $C_T = 2$ and for two values of the incidence: ———, $\alpha = 7^\circ$; — — $\alpha = 10^\circ$. (c) Geometrical shape of the membrane for $M_\infty = 2$, $\alpha = 7^\circ$ and for two values of the tension coefficient: ———, $C_T = 2$; — — $C_T = 4$.

where $\Delta p = p_m^{n+1/2} - p_{m-1}^{n+1/2}$ and $\Delta\theta = \theta_{m-1/2}^{n+1} - \theta_{m-1/2}^{n}$ represent the pressure difference across the membrane and the change in the membrane slope angle between two consecutive Lagrange-distance lines, respectively, in which subscript $_m$ denotes the closest streamline to the upper side of the membrane. This condition on the flexible membrane has to be solved together with the flux calculation equations (11) or (12), depending on the situation, at each new $\Delta\lambda$ step.

Computations have been performed with $M_\infty = 2$ and $c = 1$, for two values of the angle of attack and tension coefficient, $\alpha = 7^\circ$ and 10° and $C_T = 2$ and 4. The results obtained are shown in Fig. 16. The effect of the incidence α on the Mach number distributions along the closest streamlines to the membrane on both sides is shown in Fig. 16a, and the effect of the incidence, α, and of the tension coefficient C_T on the computed geometrical shape of the membrane are shown in Figs. 16b and c. One can notice that the required excess length of the membrane, ε, increases with α and decreases with an increase in C_T. A typical illustration of the streamline pattern of this flow is shown in Fig. 17a, and a comparison between the analytical solution and the Lagrangian method results is shown in Fig. 17b. The initial slope angle of the membrane was the same, $\theta_0 = 3.28^\circ$, while the chord was slightly different ($c = 1$ compared to 0.9927 in the analytical and numerical methods, respectively). The excess length was also comparable, $\varepsilon_{\text{analytic}} = 0.08114$ versus $\varepsilon_{\text{numeric}} = 0.08219$. Both sets of results were found in reasonable good agreement.

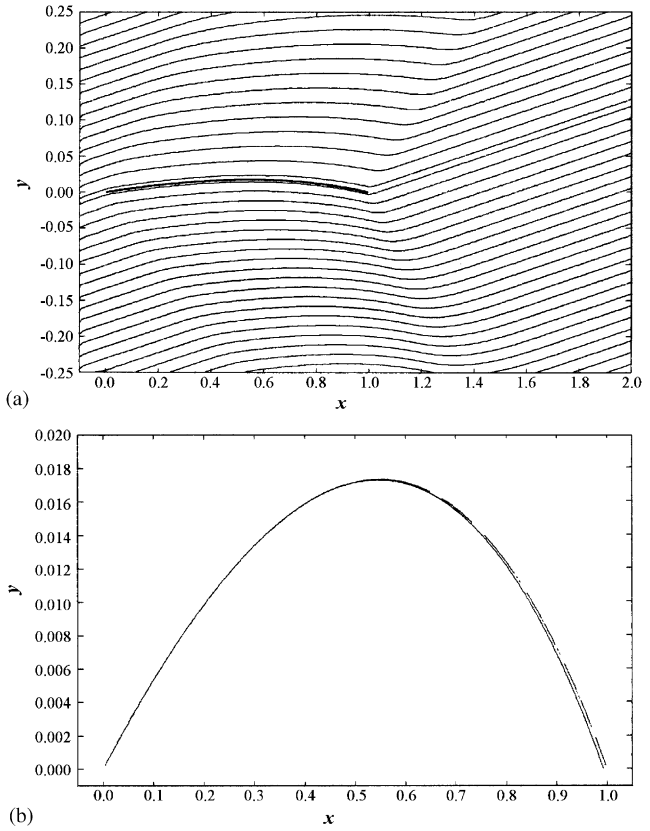

Fig. 17. Flexible-membrane airfoil. (a) Typical streamline pattern of the flow. (b) Geometrical shape of the membrane: comparison between the present Lagrangian solution (———) and the present analytical solution (— —).

5.4. *Analysis of jet-flapped airfoils*

The case of a rigid airfoil with a thin jet flap issued at its trailing edge at an angle β with respect to the chord represents another type of flow problem with geometrically unspecified boundaries. In this case, the geometry of the airfoil of chord c is specified, but the geometrical shape of the jet sheet situated along the wake depends on the jet momentum J and on the pressure difference across it (see Mateescu and Newman, 1991, for the subsonic case). In order to validate the Lagrangian solution, an analytical solution is also derived for this problem.

5.4.1. *Analytical solution*

For this airfoil flow, we will use the same notations as in Section 5.3. The pressure difference coefficient across the jet flap is determined by the same Eq. (24), obtained using the analytical method indicated in Carafoli et al. (1969). The a priori unknown slope angle θ of the jet flap is related to the pressure difference and the jet momentum, J, (as shown in Mateescu and Newman, 1991) by the equation

$$\Delta C_p = cC_J[\mathrm{d}(\tan\theta)/\mathrm{d}x], \quad C_J = 2J/(\gamma M_\infty^2 p_\infty c), \tag{32}$$

where C_J is the nondimensional jet momentum coefficient. This leads to a linear differential equation similar to Eq. (26), which can be integrated twice in order to obtain the geometrical shape of the jet flap in the form

$$\theta - \alpha = -(\beta + \alpha)\exp(-A(x/c - 1)), \quad A = 4/(BC_J), \tag{33}$$

$$h(x) = \alpha(x - c) + c\left[(\beta + \alpha)/A\right]\left[\exp(-A(x/c - 1)) - 1\right]. \tag{34}$$

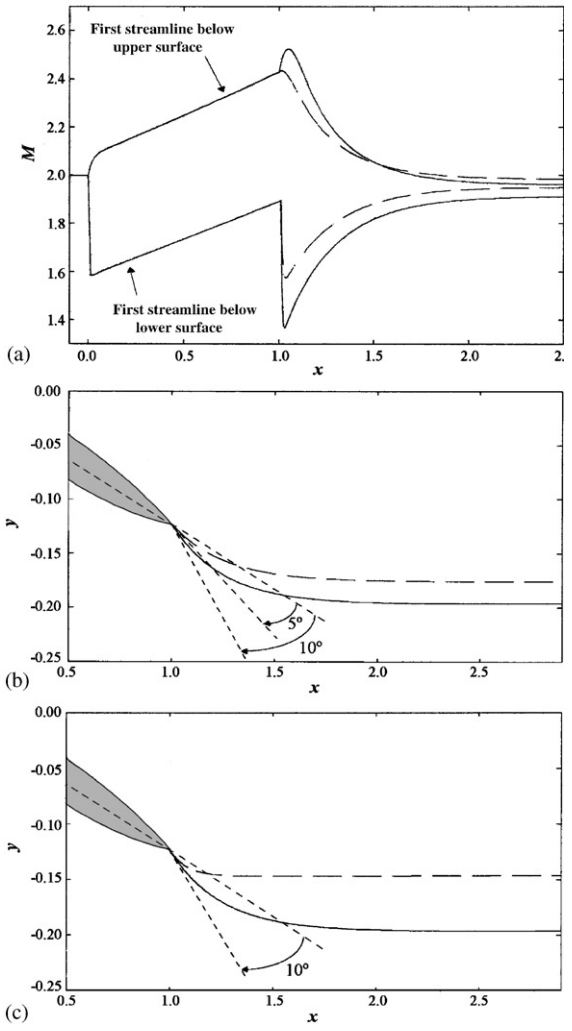

Fig. 18. *Jet-flapped airfoil*. (a) Mach number distributions along the closest streamlines to the lower and upper surface of the jet flap for $M_\infty = 2$, $\alpha = 7^\circ$, $C_J = 0.6$ and for two values of the deflection angle of the jet flap: — —, $\beta = 5^\circ$; ———, $\beta = 10^\circ$. (b) Geometrical shape of the jet flap for $M_\infty = 2$, $\alpha = 7^\circ$, $C_J = 0.6$ and for two values of the deflection angle of the jet flap: — —, $\beta = 5^\circ$; ———, $\beta = 10^\circ$. (c) Geometrical shape of the jet flap for $M_\infty = 2$, $\alpha = 7^\circ$, $\beta = 10^\circ$ and for two values of the jet-momentum coefficient: — —, $C_J = 0.2$; ———, $C_J = 0.6$.

5.4.2. *Lagrangian method solution*

In this case, the implementation of the boundary condition on the jet flap should include the equilibrium equation normal to the membrane, which can be expressed, for numerical use, as

$$\Delta\theta = 2\sin^{-1}\left(-\frac{\Delta p}{2J}\Delta\lambda\right), \quad \Delta\lambda = \lambda^{n+1} - \lambda^n, \tag{35}$$

where $\Delta p = p_m^{n+1/2} - p_{m-1}^{n+1/2}$ and $\Delta\theta = \theta_{m-1/2}^{n+1} - \theta_{m-1/2}^{n}$ represent the pressure difference across the jet flap and, respectively, the change in its slope angle between two consecutive Lagrange-distance lines (subscript $_m$ denotes the closest streamline to the upper side of the jet flap). This condition on the jet flap has to be solved together with the flux calculation equations (11) or (12) at each new $\Delta\lambda$ step.

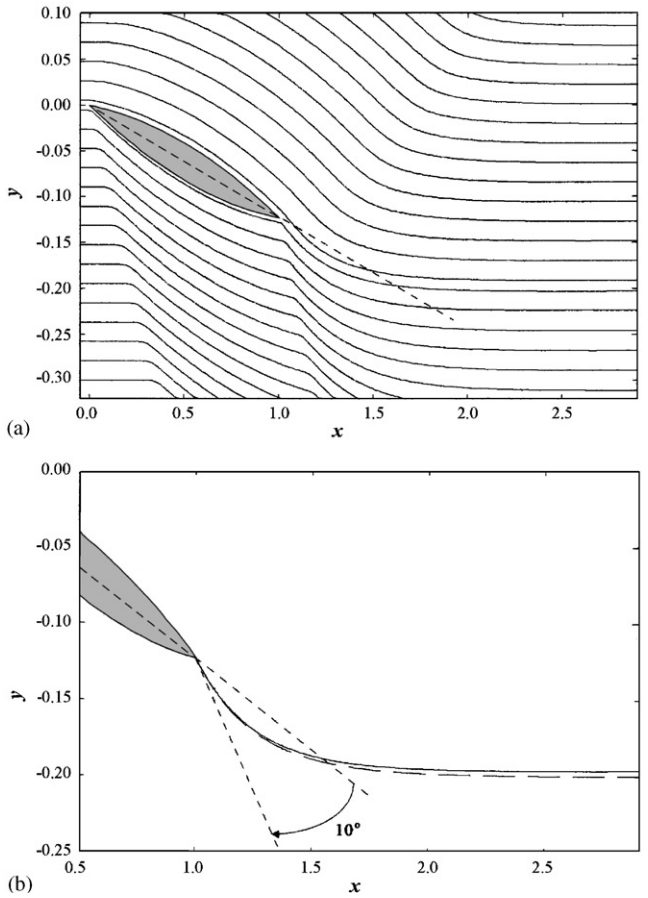

Fig. 19. *Jet-flapped airfoil*. (a) Typical streamline pattern of the flow. (b) Geometrical shape of the jet flap: comparison between the present Lagrangian solution (———) and the present analytical solution (— —).

Computations have been performed with $M_\infty = 2$ and $\alpha = 7^\circ$, considering a rigid lenticular airfoil (studied in Section 4.5) with a jet flap at a deflection angle β. The results obtained are shown in Fig. 17 for two values of the jet deflection angle, $\beta = 5^\circ$ and 10°, and for two values of the jet momentum coefficient, $C_J = 0.2$ and 0.4. The Mach number distributions along the closest streamlines to the jet flap on both sides are shown in Fig. 18a for two values of the jet deflection angle, β. The effects of the jet deflection angle β and of the jet momentum coefficient C_J on the geometrical shape of the jet flap are shown in Figs. 18b and c. A typical illustration of the streamline pattern of this flow is shown in Fig. 19a, and a comparison between the analytical solution and the Lagrangian method results is shown in Fig. 19b. A reasonable good agreement was found between these two sets of results.

6. Conclusions

An enhanced Lagrangian method has been used in this paper to solve several aerodynamic problems with geometrically unspecified geometry. This method uses the stream function and Lagrangian-distance (along the streamlines) coordinates. Two compatibility equations related to the coordinate transformation have to be simultaneously solved with the Euler equations of motion in conservation form expressed in these generalized Lagrangian coordinates; however, the continuity and energy equations reduce to constant values along the streamlines in these coordinates. The augmented system of equations is solved by integration in Lagrangian-distance (along

streamlines) using a finite volume method, in which the flux values are determined in supersonic flows based on the Riemann problem solution with a Godunov-type scheme. Special procedures have been developed in this enhanced method for a substantially improved and sharp numerical resolution of the shock waves, and for the numerical implementation of the aerodynamic conditions defining the geometrically unspecified solid or fluid boundaries.

This method has first been successfully validated for aerodynamic problems with solid boundaries of specified geometry by comparison with exact analytical solutions and with previous computational results obtained by numerical methods using Eulerian formulations.

Then this enhanced Lagrangian method has been used to determine the solution of several flow problems with geometrically unspecified boundaries: (1) Determination of the geometrical shape of an airfoil, or of a portion of a nozzle wall, corresponding to a specified pressure distribution (indirect flow problems). (2) Supersonic nozzle design problem based on the reflection-suppression condition for obtaining a specified uniform flow at the nozzle outlet (design flow problem). (3) Analysis of supersonic flows past flexible-membrane airfoils (an adaptive-structure flow problem). (4) Analysis of supersonic flows past jet-flapped airfoils (an adaptive fluid boundary problem with slip lines).

In all cases, this enhanced Lagrangian method displayed an excellent computational efficiency and led to accurate solutions with a sharp numerical resolution of the shock waves and a rigorous treatment of the expansion fans. This method displayed an excellent capability of solving very efficiently the flow problems with geometrically unspecified solid or fluid boundaries.

Acknowledgements

The support of the Natural Sciences and Engineering Council of Canada is gratefully acknowledged, as well as the contributions of his former and present graduate students L. Chocron, P. Nasrallah and C.S. Neculita to the computation and graphical representation of the results for many numerical examples presented in the paper.

References

Anderson Jr., J.D., 1991. Modern Compressible Flow with Historical Perspective. McGraw Hill, New York.

Anderson, W.K., Thomas, J.L., Vanleer, B., 1986. Comparison of finite volume flux vector splittings for the Euler equations. AIAA Journal 24, 1453–1460.

Carafoli, E., Mateescu, D., Nastase, A., 1969. Wing Theory in Supersonic Flow, Pergamon Press, Oxford.

Eidelman, S., Colella, P., Shreeve, R.P., 1984. Application of the Godunov method and its second order extension to cascade flow modeling. AIAA Journal 22, 1609–1615.

Glatz, H.M., Wardlaw, A.B., 1984. A higher-order Godunov scheme for steady supersonic gas dynamics. Journal of Computational Physics 58, 157–187.

Hui, W.H., Zhao, Y.C., 1993. A generalized Lagrangian method for solving the Euler equations. In: Donato, A., Oliveri, F. (Eds.), Proceedings of the Fourth International Conference on Hyperbolic Problems.

Liou, M.-S., 1995. An extended Lagrangian method. Journal of Computational Physics 118, 294–309.

Loh, C.Y., Hui, W.H., 1991. A new Lagrangian method for steady supersonic flow computation, Part 1: Godunov scheme. Journal of Computational Physics 82, 207–240.

Loh, C.Y., Hui, W.H., 1993. Lagrangian random choice method for steady two dimensional supersonic/hypersonic flow. AIAA Journal 31, 2193–2194.

Loh, C.Y., Liou, M.-S., 1993. Lagrangian solution of supersonic real gas flow. Journal of Computational Physics 104, 150–161.

Loh, C.Y., Liou, M.-S., 1994. A new Lagrangian method for three-dimensional steady supersonic flows. Journal of Computational Physics 113, 224–248.

Mateescu, D., 1987. Wing and conical body of arbitrary cross-section in supersonic flow. Journal of Aircraft 24 (4), 239–247.

Mateescu, D., 1990. A hybrid panel method for aerofoil aerodynamics. In: Boundary Element XII, Vol. 2. Springer, Berlin and New York, pp. 3–14.

Mateescu, D., Chocron, L., 1996. Solutions for jet-flapped airfoils and aerodynamic nozzle design based on a Lagrangian computational method. Proceedings of the 15th International Conference on Numerical Methods in Fluid Dynamics, Monterey, CA, pp. 254–255.

Mateescu, D., Nasrallah, P., 1995. Computational solutions based on a Lagrangian formulation for aerodynamic problems of unspecified geometry. In: Carlomagno, G.M., Brebbia, C.A. (Eds.), Computational Methods and Experimental Measurements, Vol. VII. Computational Mechanics Publications, Southampton and Boston, pp. 317–325.

Mateescu, D., Newman, B.G., 1991. Analysis of flexible-membrane and jet-flapped airfoils using velocity singularities. AIAA Journal of Aircraft 28, 789–795.

Mateescu, D., Stanescu, D., 1995. A biased flux method for solving the Euler equations in subsonic, transonic and supersonic flows. In: Carlomagno, G.M., Brebbia, C.A. (Eds.), Computational Methods and Experimental Measurements, Vol. VII. Computational Mechanics Publications, Southampton and Boston, pp. 327–335.

Mateescu, D., Venditti, D.A., 2001. Unsteady confined viscous flows with oscillating walls and multiple separation regions over a downstream-facing step. Journal of Fluids and Structures 15, 1187–1205.

Ni, R.H., 1982. A multiple-grid scheme for solving the Euler equations. AIAA Journal 20, 1565–1571.

Roe, P.L., 1986. Discrete models for the numerical analysis of time-dependent multidimensional gas dynamics. Journal of Computational Physics 63, 458–476.

Strain, J., 1999. Semi-Lagrangian methods for level set equations. Journal of Computational Physics 151, 498–533.

Strain, J., 2001. A fast semi-Lagrangian method for moving interfaces. Journal of Computational Physics 151, 498–533.

Van Roessel, H.J., Hui, W.H., 1989. A Lagrangian formulation for steady three-dimensional Newton–Busemann flow. Journal of Applied Mathematics and Physics 40, 677–710.

Yang, J.Y., Hsu, C.A., 1993. Solution of the steady Euler equations in a generalized Lagrangian formulation. AIAA Journal 31, 266–272.

Yang, J.Y., Chang, S.H., Hui, W.H., 1993. New Lagrangian method for steady supercritical shallow water flow computation. Computer Methods in Applied Mechanics and Engineering 104, 333–355.